sustainability

MDPI

Article

Ammonia as a Marine Fuel towards Decarbonization: Emission Control Challenges

Georgia Voniati, Athanasios Dimaratos, Grigorios Koltsakis * and Leonidas Ntziachristos

Laboratory of Applied Thermodynamics, Department of Mechanical Engineering, Aristotle University of Thessaloniki, 54124 Thessaloniki, Greece; voniatig@meng.auth.gr (G.V.); adimaratos@auth.gr (A.D.); leon@auth.gr (L.N.)

* Correspondence: grigoris@auth.gr

Abstract: Decarbonization of the maritime sector to achieve ambitious IMO targets requires the combination of various technologies. Among alternative fuels, ammonia (NH_3), a carbon-free fuel, is a good candidate; however, its combustion produces NO_x, unburnt NH_3 and N_2O—a strong greenhouse gas (GHG). This work conducts a preliminary assessment of the emission control challenges of NH_3 application as fuel in the maritime sector. Commercial catalytic technologies are applied in simulated NH_3 engine exhaust to mitigate NH_3 and NO_x while monitoring N_2O production during the reduction processes. Small-scale experiments on a synthetic gas bench (SGB) with a selective-catalytic reduction (SCR) catalyst and an ammonia oxidation catalyst (AOC) provide reaction kinetics information, which are then integrated into physico-chemical models. The latter are used for the examination of two scenarios concerning the relative engine-out concentrations of NO_x and NH_3 in the exhaust gas: (a) shortage and (b) excess of NH_3. The simulation results indicate that NO_x conversion can be optimized to meet the IMO limits with minimal NH_3 slip in both cases. Excess of NH_3 promotes N_2O formation, particularly at higher NH_3 concentrations. Engine-out N_2O emissions are expected to increase the total N_2O emissions; hence, both sources need to be considered for their successful control.

Keywords: shipping; decarbonization; GHG; ammonia; emission control; NO_x; N_2O

Citation: Voniati, G.; Dimaratos, A.; Koltsakis, G.; Ntziachristos, L. Ammonia as a Marine Fuel towards Decarbonization: Emission Control Challenges. *Sustainability* **2023**, *15*, 15565. https://doi.org/10.3390/su152115565

Academic Editor: Dino Musmarra

Received: 1 September 2023
Revised: 19 October 2023
Accepted: 30 October 2023
Published: 2 November 2023

1. Introduction

Maritime transport, mainly powered by diesel engines, is responsible for almost 3% of global greenhouse gas (GHG) emissions, which is expected to further increase until 2050 [1]. Apart from GHGs, the maritime sector accounts for 24% of nitrogen oxides (NO_x), 24% of sulfur oxides (SO_x) and 9% of particulate matter (PM) emissions in the European Union (EU) [2].

According to the initial IMO strategy, GHG emissions shall be reduced by at least 50% by 2050 and carbon intensity by 40% by 2030 compared to 2008, aiming at complete decarbonization of maritime transport by 2100 [3]. The latest meetings of the IMO Marine Environment Protection Committee (MEPC) recently adopted a revised strategy that aims at net-zero GHG emissions by 2050 [4]. This is a notable acceleration in the emission reduction efforts compared to the initial IMO strategy. In parallel, NO_x emissions shall comply with Tier III limits (3.4 g/kWh for vessel propelled by low-speed two-stroke engines) in Emission Control Areas (ECAs) and Tier II (14.4 g/kWh for vessel propelled by low-speed two-stroke engines) globally. Concerning SO_x emissions, IMO has introduced the global sulfur cap, which imposes an upper limit of 0.50% in the fuel sulfur content globally, dropping to 0.10% in Sulfur Emission Control Areas (SECAs) [5].

Moving towards this direction, several technologies and strategies have already been implemented or are currently being developed, such as [6]:

- direct reduction in fuel consumption, e.g., operating strategies and route optimization as well as slow steaming;

- direct reduction in vessel resistance, e.g., air lubrication, optimized hull design and coating, lightweight materials;
- alternative propulsion system and power sources, e.g., wind-assisted propulsion, fuel cells, cold ironing;
- improvement of energy efficiency, e.g., propulsion system hybridization, waste heat recovery;
- post-combustion gas treatment, e.g., CO_2 capture

Another way to reduce carbon intensity of shipping is the application of alternative fuels with low or zero carbon content, produced using sustainable sources and feedstock and renewable energy (often referred as e-fuels or green fuels). Some alternative fuels (e.g., biofuels) can be used directly on existing engines (drop-in fuels), while others (e.g., ammonia, hydrogen) require significant developments and modifications before becoming the main energy source on board the vessel. Although the combination of various technology packages and practices can reach significant reductions of GHG emissions, complete decarbonization can be achieved only when using carbon-neutral fuels [6,7].

Among other alternative fuels with low or zero carbon content (LNG, LPG, methanol, hydrogen, etc.), ammonia (NH_3) is a promising solution to limit carbon (C) and sulfur (S) emissions from the maritime sector due to several advantages, such as absence of C and S atoms from its molecule, high energy density and relatively easy storage. However, the poor combustion properties of NH_3 (low flammability, high autoignition temperature, low flame speed, etc.) create the need of a pilot fuel quantity, usually carbonaceous, for initiating combustion [8–11]. Depending on the pilot fuel used, there may be carbon dioxide (CO_2), SO_x and PM emissions, but these levels should be very low (or almost negligible) compared to conventional fuels (particularly heavy fuel oil (HFO)).

Moreover, NH_3 combustion produces three main emission species that have a significant impact on human health and climate: unburned NH_3 that is highly toxic and can cause several health issues when found in high concentrations; NO_x, which is one of the main air pollutants and nitrous oxide (N_2O) [9], a GHG with global warming potential (GWP) almost 300 times higher than that of CO_2, over a 100-year period [12]. Consequently, even small concentrations of N_2O potentially decrease the benefit from CO_2 reduction [13]. Nitrous oxide (N_2O) is a potential byproduct of both NH_3 in-cylinder combustion and chemical reactions in the exhaust gas aftertreatment system. Unburned NH_3 and NO_x emissions can be expected from an engine running on NH_3 and can be reduced using catalytic devices that are commercially available. In marine applications, a vanadium-based selective catalytic reduction (V-SCR) system is commonly used to reduce NO_x with NH_3 or urea as reducing agent [14,15]. Ammonia slip (i.e., unreacted NH_3 downstream of the SCR system) exceeding the need of the deNO_x process can be minimized with an ammonia slip catalyst (ASC). Although that reduction of NH_3 can promote NO_x and N_2O formation [16], N_2O may also be formed in lower concentrations through the SCR reactions [17,18]. Catalytic N_2O reduction technologies are already available but are customized for other applications such as chemical industries and stationary combustion [19,20]. As reduction of a specific species can promote the formation of another, the design of the exhaust after-treatment system (EATS) for an engine running on NH_3 is expected to consist of multiple emission control technologies.

Based on the above, it is clear that commercial technologies must be developed and adopted to effectively reduce NH_3 slip, NO_x and N_2O at the same time in the NH_3 engine exhaust. However, NH_3 engines (particularly large two-stroke ones used in the maritime sector) are not yet commercially available; therefore, the exact exhaust gas conditions in terms of composition, temperature and flow rate needed for the design of an emission control system are not precisely known. Even when the exhaust gas of the NH_3 engine is known from measurements, the design of emission control via trial and error is prohibitive in view of the huge testing costs on a large two-stroke marine engine. It is therefore imperative to develop accurate and predictive models of the aftertreatment system that will be applicable in a wide range of conditions to ensure the coverage of all possible scenarios

to be expected in a real NH_3 engine exhaust. The development of such a model is actually the main target of the present work.

The current study presents the development of simulation models of the aftertreatment system of NH_3 application as a fuel in the maritime sector. The primary aim is to determine the viability of current catalytic technologies, identify emission control challenges and ultimately guide the optimum design at an early phase. Exhaust aftertreatment models rely on kinetic mechanisms and rate expressions that describe the intrinsic chemical properties of the active materials. In this work, experiments are performed to derive the respective kinetic information for two technologies of interest and introduce them in an integrated physico-chemical model of the transient transport and reaction processes in monolithic catalytic reactors. The model is then used to study two possible scenarios concerning the proportion of NH_3 and NO_x emissions from NH_3 combustion (engine-out conditions). The first scenario assumes that engine-out NH_3 is less than NO_x ($NH_3/NO_x < 1$), so additional NH_3 has to be injected upstream of a V-SCR catalyst to achieve NO_x levels below Tier III limits. The second scenario examines the case of excess engine-out NH_3 ($NH_3/NO_x > 1$) where a dual layer ASC (SCR on top of an ammonia oxidation catalyst (AOC) layer) is integrated to the aftertreatment system to handle the NH_3 slip. Particular emphasis is given to the formation of N_2O through NO_x and NH_3 catalytic reduction.

2. Materials and Methods

2.1. Experimental

Two small-scale samples of commercial catalysts are used in the experimental part of this study: (1) a V-SCR (commonly used in marine applications) with a diameter of 28 mm and a length of 90 mm and (2) a platinum-based AOC with the same dimensions. Their catalytic activity is evaluated with measurements on a synthetic gas bench (SGB), presented in Figure 1. The flow and composition of the mixture is controlled by the programmable mass flow controllers (MFCs). Moisture can be added to the mixture through an H_2O feed, which is heated beforehand to prevent condensation of the flue gas. The mixture is then heated to the required temperature through a pre-heater system before passing through the catalyst sample. The bypass line gives the flexibility to conduct operational and calibration checks of the analyzers, as well as to determine the exhaust gas composition without exposing the catalyst to the gas mixture. An FTIR gas analyzer (AVL Sesam i60 FT SII Small) measures the concentrations of all species in the outlet gas.

In the present work, the SCR and AOC reaction mechanisms are studied by running targeted experimental protocols. For the SCR, steady-state measurements are performed at temperatures between 150 °C and 500 °C and at atmospheric pressure. In the case of AOC, its activity is tested by a temperature ramp (light-off test) from 150 °C to 600 °C under atmospheric pressure. The test conditions for the SCR and AOC testing are summarized in Tables 1 and 2, respectively.

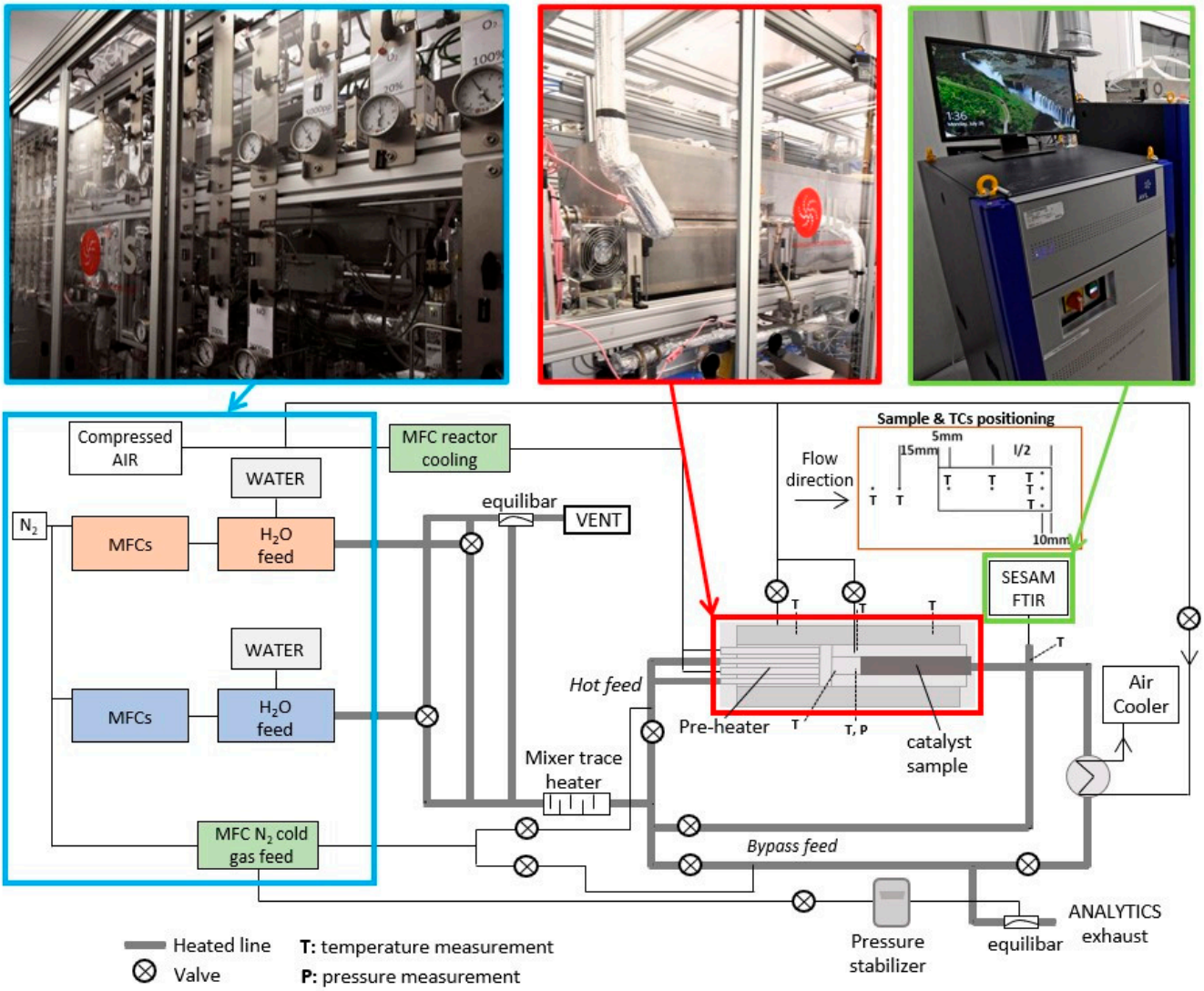

Figure 1. Small-scale experimental setup of synthetic gas bench (SGB).

Table 1. SCR experimental conditions.

Phenomena	Inlet Feed Gas	Temperature [°C]	Space Velocity [h^{-1}]
NO oxidation	2000 ppm NO, 6% O_2, 15% H_2O, 15 ppm SO_2, N_2 balance	150 200 250 300 400 500	20,000
NH_3 oxidation	1000 ppm NH_3, 6% O_2, 15% H_2O, 15 ppm SO_2, N_2 balance		
Standard SCR	2000 ppm NH_3, NH_3/NO_x = 0.8, 1, 1.5, 6% O_2, 15% H_2O, 15 ppm SO_2, N_2 balance		
Fast SCR	2000 ppm NH_3, 2000 ppm NO_x (NO_2/NO_x = 0.2), 6% O_2, 15% H_2O, 15 ppm SO_2, N_2 balance		

Table 2. AOC experimental conditions.

Phenomena	Inlet Feed Gas	Temperature [°C]	Space Velocity [h^{-1}]
NH_3 oxidation	250 ppm NH_3, 50 ppm NO, 6% O_2, 15% H_2O, 15 ppm SO_2, N_2 balance	150 → 600	20,000

2.2. Modeling

2.2.1. Main Assumptions and Governing Equations

The kinetic mechanisms of the V-SCR and Pt-AOC are implemented into a model of the ExothermiaSuite® simulation platform [21]. The monolith is simulated as a single representative channel (1D simulation approach), assuming that the inlet flow distribution is uniform and heat losses are negligible. Temperature and species concentrations are computed by solving the quasi-steady state balance equations for heat (Equation (1)) and mass (Equation (2)) transfer:

$$\rho_g C_{p,g} v_g \frac{\partial T_g}{\partial z} = -h \times \left(\frac{S_F}{\varepsilon}\right) \times \left(T_g - T_s\right) \tag{1}$$

$$\frac{\partial\left(v_g y_{g,j}\right)}{\partial z} = -k_j \times \left(\frac{S_F}{\varepsilon}\right) \times \left(y_{g,j} - y_{s,j}\right) \tag{2}$$

The wall surface temperature is calculated using the transient energy balance in the solid phase (Equation (3)):

$$\rho_s C_{p,s} \frac{\partial T_s}{\partial t} = \lambda_{s,z} \frac{\partial^2 T_s}{\partial z^2} + S \tag{3}$$

The surface concentrations are obtained by solving the concentration field inside the washcoat layer (Equation (4)):

$$-D_{w,j} \frac{\partial^2 y_{s,j}}{\partial w^2} = \sum_k n_{j,k} R_k \tag{4}$$

The convective mass transfer from the gas to the washcoat surface is formulated as

$$\frac{\partial\left(v_g y_{g,j}\right)}{\partial z} = k_j \left(\frac{S_F}{\varepsilon}\right) \left(y_{s,j}\Big|_{w=-w_c} - y_{g,j}\right) \tag{5}$$

Supplementary equations regarding the model of the flow through catalyst are provided in Appendix A.

The solution of the concentration field in the washcoat layer is of particular importance for the case of technologies with multiple catalytic layers (1D + 1D model). In fact, this is the case with ASCs that usually contain both a precious metal (PGM) layer, particularly an AOC layer for the oxidation of NH_3, as well as an SCR layer on top (Figure 2). This combination comes with advantages concerning NH_3 reduction and selectivity properties of the ASC, as NO_x formed in the oxidation layer diffuses through the SCR layer where it can be reduced [14].

2.2.2. Reaction Mechanisms

In order to examine the potential of the existing catalytic devices to treat NH_3 combustion products, thoroughly calibrated and validated SCR and AOC models are necessary. To describe the SCR reactivity over the vanadium-based catalyst, commonly used SCR reactions are adopted [16,22], as listed in Table 3. The standard, fast and NO_2 SCR reactions are considered the principal reactions between NO_x and NH_3 (depending on the proportion

of NO_2/NO_x). While NH_3 is primarily oxidized to N_2, oxidation reactions to NO and N_2O are also considered. The formation of N_2O has also been attributed to the oxidation of NH_3 and NO [23], as well as to the direct reaction between NH_3 and NO_2 [24,25].

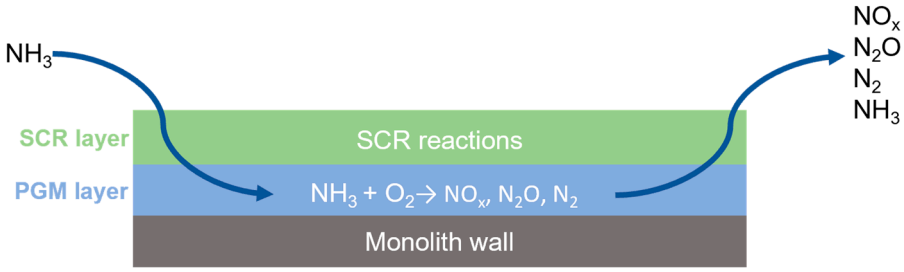

Figure 2. Dual-layer ASC schematic configuration.

Table 3. SCR reaction scheme.

Type	Reaction
NH_3 storage/release	$NH_3 \leftrightarrow NH_3$ *
Standard SCR	$4\ NH_3 * + 4\ NO + O_2 \rightarrow 4\ N_2 + 6\ H_2O$
Fast SCR	$4\ NH_3 * + 2\ NO + 2\ NO_2 \rightarrow 4\ N_2 + 6\ H_2O$
NO_2 SCR	$NH_3 * + 3/4\ NO_2 \rightarrow 7/8\ N_2 + 3/2\ H_2O$
N_2O formation	$2\ NH_3 * + 2\ NO + O_2 \rightarrow N_2 + N_2O + 3\ H_2O$ $4\ NH_3 * + 4\ NO_2 \rightarrow 2\ N_2 + 2\ N_2O + 6\ H_2O$
NO oxidation	$NO + 1/2\ O_2 \leftrightarrow NO_2$
NH_3 oxidation	$4\ NH_3 * + 5\ O_2 \rightarrow 4\ NO + 5\ H_2O$ $2\ NH_3 * + 3/2\ O_2 \rightarrow N_2 + 3\ H_2O$ $4\ NH_3 * + 4\ O_2 \rightarrow 2\ N_2O + 6\ H_2O$

* Stored NH_3 on the catalyst sites.

Ammonia oxidation on the platinum-based AOC is approached with a simple kinetic model that can give good representation of the overall reactions. The oxidation reactions used are listed in Table 4. These include the oxidation of NH_3 to N_2 and NO, the simultaneous oxidation of NH_3 and NO to N_2O and the oxidation of NO to NO_2 (including the reverse reaction of NO_2 decomposition) [26,27].

Table 4. AOC reaction scheme.

Type	Reaction
NO oxidation	$NO + 1/2\ O_2 \leftrightarrow NO_2$
NH_3 oxidation	$4\ NH_3 + 5\ O_2 \rightarrow 4\ NO + 5\ H_2O$ $2\ NH_3 + 3/2\ O_2 \rightarrow N_2 + 3\ H_2O$
NH_3 and NO oxidation to N_2O	$2\ NH_3 + 2\ NO + 3/2\ O_2 \rightarrow 2\ N_2O + 3\ H_2O$

2.3. Full-Scale Application of the Model

Assumptions and Inlet and Boundary Conditions

The target of this section is to demonstrate the use of modeling in the design phase of the NH_3 marine engine exhaust aftertreatment system. In the early design phase, many parameters that influence the catalyst selection and optimization are not known, including NO_x, NH_3 and N_2O engine-out emission levels. Here, it is assumed that the engine will use small amounts of pilot fuel [9,28,29]; therefore, CO_2 emissions can be neglected, at least at the preliminary design of the EATS. Although engine-out N_2O produced by NH_3 combustion is a topic of high concern [28,30], for the purposes of the present work it will also be considered negligible; nevertheless, the N_2O that is potentially produced in the

EATS as an unwanted byproduct will be examined, and its greenhouse effect potential will be evaluated.

Ammonia combustion is likely to produce high levels of unburnt NH_3 [29,30], resulting in concentrations comparable to the respective NO_x emissions in terms of mole fraction. It is well known that the molar ratio of NH_3/NO_x in the exhaust gas is very critical for the operation of the SCR. Ratios below 1 would probably necessitate extra NH_3 in the exhaust gas stream, eventually via an additional NH_3 injection system. On the other hand, if the ratio is above 1, then the excess NH_3 escaping the SCR reactions will have to be treated by dedicated catalysis.

In this preliminary concept study, both cases described above will be studied. In the first case, NH_3 injection upstream of a V-SCR is required as shown in Figure 3a. In the second case, a dual layer/dual function ASC is placed downstream from the SCR (Figure 3b) to treat the unreacted NH_3 of the deNO_x process. The ASC is assumed to be a combination of V-based (SCR) and precious-metal based catalytic layers (AOC) (as shown indicatively in Figure 2) in order to attain a desired NH_3 oxidation selectivity to N_2.

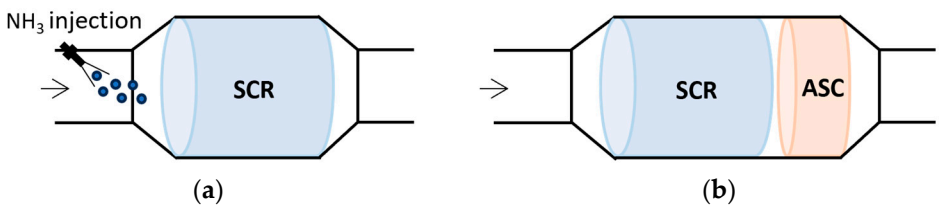

Figure 3. Model exhaust layouts for the two cases examined here: (**a**) shortage of NH_3 and (**b**) excess of NH_3 in the exhaust gas.

Since NH_3 engines are currently under development and their real exhaust gas conditions and emission concentrations are still not known precisely, the current study is based on real-world engine-out conditions of low-speed diesel engines used in marine applications, assuming a high-pressure (pre-turbo) SCR system [31,32]. The simulated catalyst inlet conditions are summarized in Table 5. Pre-turbo SCR configurations have the advantage of higher pressures and temperatures that prevail right after the engine and expand the active range of SCR operation, especially in low loads [33,34]. It is worth noting that the physico-chemical model can be applied in the entire operating envelope and is sensitive to the effect of pressure on reaction rates and species diffusivity.

Table 5. Exhaust gas conditions assumed in this study.

Engine Load	**%**	**100**	**75**	**50**	**25**
Exhaust gas temperature	°C	410	350	310	290
Exhaust gas pressure	bar	4.0	3.1	2.1	1.4
SCR space velocity	h^{-1}	40,000	32,000	25,000	10,000
ASC space velocity	h^{-1}	140,000	115,000	85,000	40,000
NO_x concentration	ppm	1500–2000	1500–2000	1500–2000	1500–2000

3. Results

3.1. Reaction Model Calibration

The reaction kinetic parameters of the two catalysts are calibrated to fit the experimentally determined NO_x, NH_3 and N_2O concentrations. The results of the NO and NH_3 oxidation tests for the V-SCR catalyst (see Table 1) are presented in Figure 4 with markers. Oxidation of NO to NO_2 is hardly detected even at high temperatures (Figure 4a). NH_3 is mainly oxidized to N_2 above 300 °C and is almost fully oxidized at 500 °C (Figure 4b), while NO and N_2O formation is observed only at very high temperatures (500 °C). The same figures contain the results of the simulation model after fitting of the reaction kinetic

rate parameters. The model achieves a good agreement with the test results in the whole temperature range and is able to predict the reaction selectivity towards NO and N_2O.

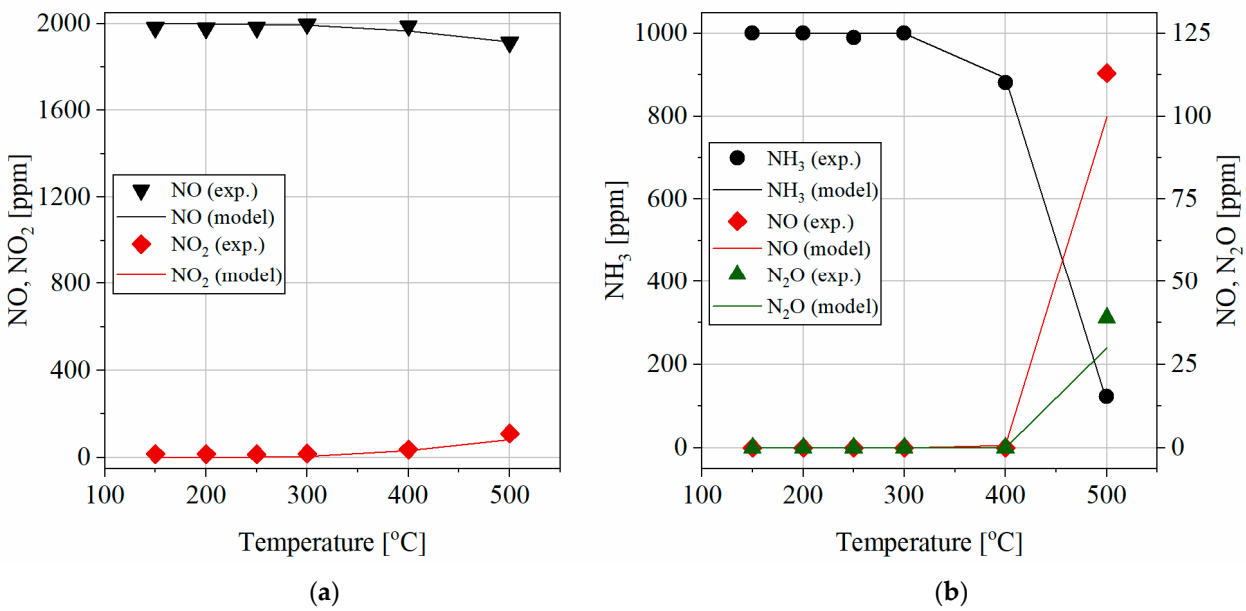

Figure 4. Comparison of experimental data (symbols) and the model (solid lines) of (**a**) NO oxidation and (**b**) NH_3 oxidation, over the V-SCR.

The results of the SCR activity tests presented in Figure 5 show that the catalyst exceeds 80% NO_x conversion above 300 °C. Obviously, the SCR process is highly dependent on the amount of NH_3 in the feed gas (Figure 5a). When the NH_3/NO_x ratio is greater than 1, NO_x is almost fully converted at high temperatures, although this leads to unreacted ammonia. When the NH_3/NO_x ratio is less than 1, only partial NO_x conversion is achieved as expected from the reaction stoichiometry (Standard SCR reaction (Table 3)). Addition of NO_2 in the feed gas (Figure 5b) enhances NO_x conversion rates, especially at low temperatures. Low selectivity to N_2O (below 20 ppm) is observed in all conditions with a significant increase of up to 120 ppm at 500 °C.

The results of the calibrated simulation model presented in the above figures with lines clearly show a good agreement with the respective measured data in the whole range of temperature, NH_3/NO_x ratio and NO_2/NO_x ratio conditions.

Figure 6 shows the axial profiles of NO_x, NH_3 and N_2O along the V-SCR catalyst as well as the reaction rates governing N_2O formation pathways. One can observe that N_2O attains stabilization approximately midway through the catalyst length, whereas NO_x and NH_3 concentrations reach a state of equilibrium near the catalyst outlet. This is attributed to the constrained availability of NH_3 and NO_x in the feed gas; hence, the reaction rates that favor N_2O formation are minimized midway through the catalyst.

The results of the Pt-based AOC tests are summarized in Figure 7. Here, the focus is not only on the conversion rate of NH_3 as a function of temperature, but also on the unwanted NO_x and N_2O produced by the NH_3 oxidation reactions. It is worth noting that the calibrated model is capable of capturing these complex trends with respect to NO_x byproducts in the whole temperature range with good accuracy. This provides the basis for using this physico-chemical model in the conditions expected in a real marine engine.

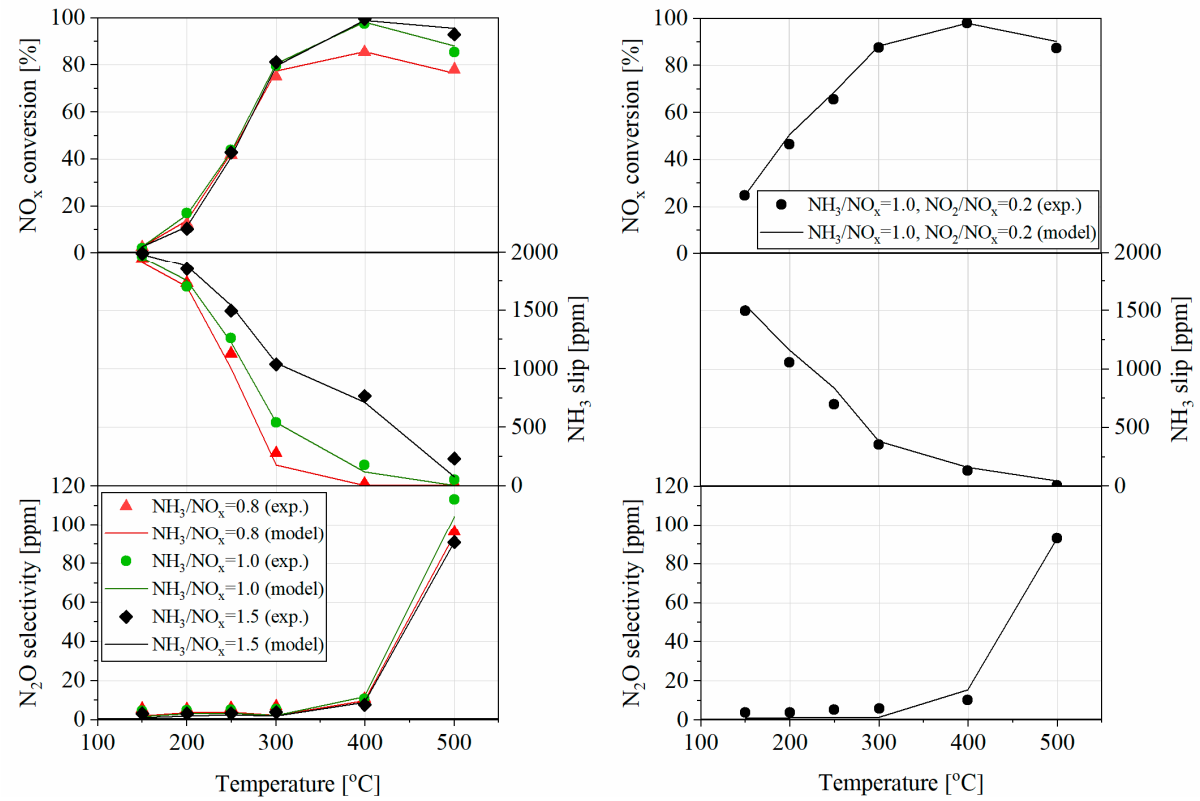

(**a**) (**b**)

Figure 5. NO_x conversion, NH_3 slip and N_2O formation over the V-SCR under (**a**) standard SCR conditions with NH_3/NO_x = 0.8, 1.0, 1.5 and NO_2/NO_x = 0 and (**b**) fast SCR conditions with NH_3/NO_x = 1.0 and NO_2/NO_x = 0.2, based on the experimental data (symbols) and the model (solid lines).

The concentration of NH_3 shows a steep decrease from 200 °C to 250 °C and is fully oxidized around 300 °C. Above 200 °C, N_2O selectivity increases significantly with maximum concentration at 250 °C. Selectivity to NO and NO_2 is favored at temperatures above 250 °C, while N_2O selectivity is simultaneously decreasing. It is important to highlight the temperature range of N_2O formation (in the aftertreatment system) between 200 °C and 400 °C, which is crucial for low-speed marine engines since their exhaust gas temperature falls within this range (see Table 5). The trends can be interpreted by referring to the reaction rates depicted in Figure 8, highlighting the competition between the reactions. Between 200 °C and 400 °C, the simultaneous oxidation of NH_3 and NO to N_2O is favored, while above 250 °C the oxidation of NH_3 to NO becomes dominant; hence, the availability of NH_3 towards N_2O is limited.

Figure 9 presents the axial distribution of NH_3, NO and N_2O along the AOC. At notably low temperatures (i.e., 150 °C), oxidation reactions governing the AOC are not activated; therefore, no alteration in emission levels is observed. Conversely, at elevated temperatures (i.e., 350 °C and 500 °C), NH_3 experiences complete oxidation in close proximity to the catalyst inlet, precluding its availability for subsequent oxidation pathways towards NO and N_2O. Consequently, NO and N_2O levels exhibit an early stabilization along the catalyst length.

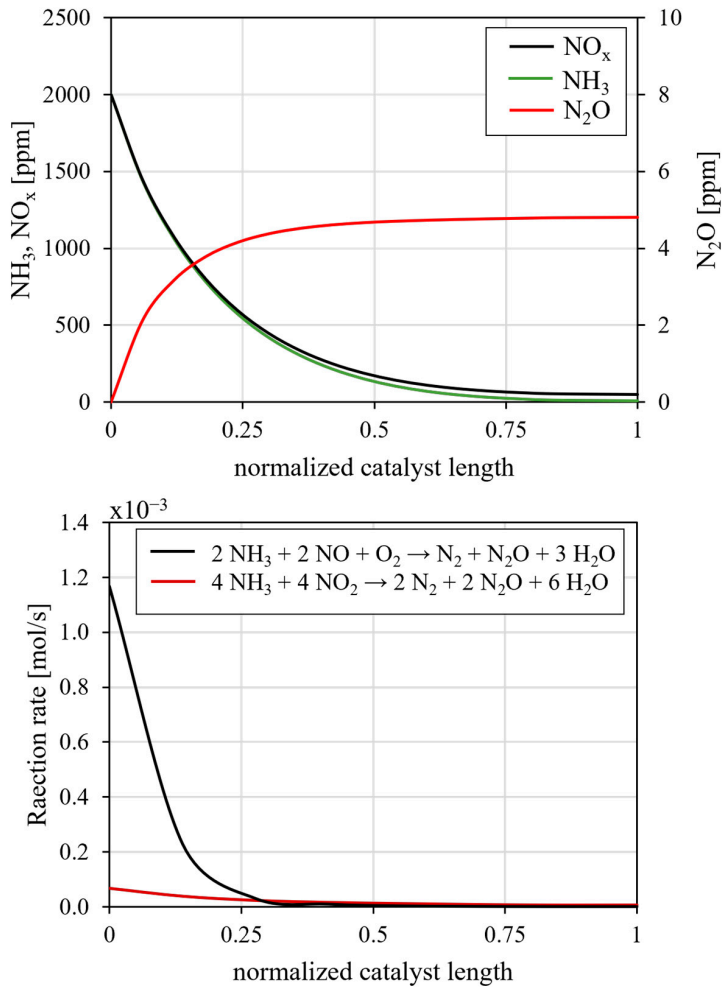

Figure 6. Concentrations of NO_x, NH_3 and N_2O as functions of axial positions along the V-SCR catalyst (**top**) and reaction rates of the N_2O pathways (**bottom**) at NH_3/NO_x = 1.0 and 400 °C.

3.2. Model Application in Marine Engine Exhaust

Based on the assumed marine engine exhaust gas conditions of Table 5 and the weighting factors of the legislated E3 test cycle [35], it can be estimated that the NO_x conversion efficiency required to reduce large two-stroke engine-out emissions below the Tier III limit of 3.4 gNO_x/kWh is in the order of 90%.

In the case of lack of NH_3 (engine-out $NH_3/NO_x < 1$), where only the SCR catalyst is used (Figure 3a), the minimum $deNO_x$ requirement may be achieved provided that NH_3 is injected with a target ratio of NH_3/NO_x equal to 0.9.

Applying the simulation model at the four loads of the E3 cycle, using the conditions shown in Table 5, NH_3 slip and N_2O formation after the SCR are calculated, as presented in Figure 10a. Almost all NH_3 is predicted to be consumed during NO_x reduction, leading to limited NH_3 slip of less than 5 ppm. Low levels of N_2O (below 8 ppm) are expected to be formed at all loads with increased selectivity at full load as N_2O formation is favored at elevated temperatures. Despite its low selectivity, N_2O is a strong GHG with 100-year GWP almost 300 times higher than CO_2. Hence, even small concentrations of N_2O can be equivalent to significant CO_2 emissions. In this case, the CO_2-equivalent emissions over a 100-year period reach almost 25 g/kWh at 100% load, which are decreased at lower loads (Figure 10b), resulting in an average value of 14.1 gCO_2-eq/kWh (taking into account the weighting factors of the E3 test cycle [28]).

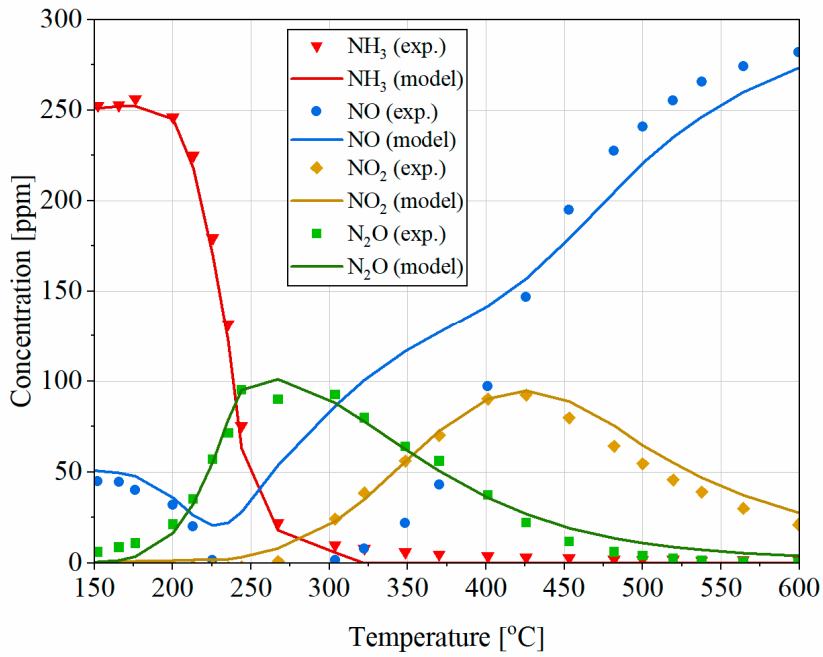

Figure 7. Comparison of the NH_3, NO_x, NO_2 and N_2O outlet concentrations for NH_3 over the AOC based on the experimental data (symbols) and the model (solid lines).

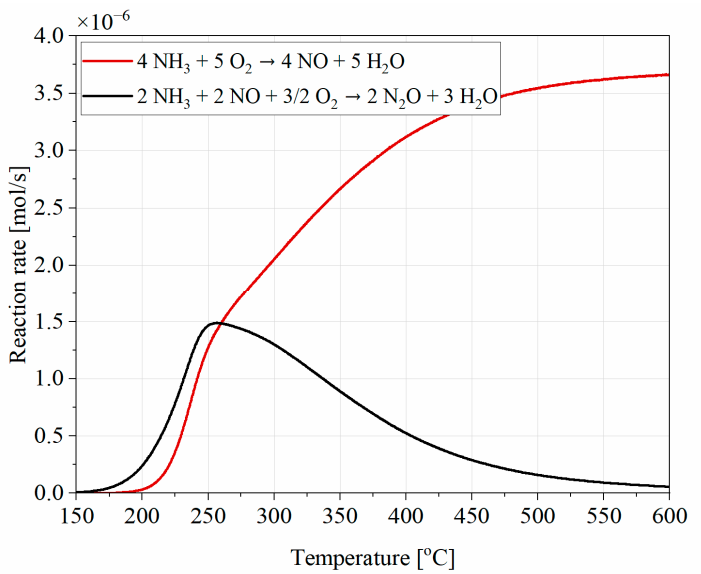

Figure 8. Reaction rates of the oxidation reactions of AOC as a function of the catalyst temperature.

Figure 11 presents the average NH_3, NO_x, N_2O and CO_2-equivalent emissions for different NH_3/NO_x ratios in the case of excess engine-out NH_3 ($NH_3/NO_x > 1$). All concentrations are estimated taking into account the weighting factors of each load according to the E3 test cycle [35]. According to the standard SCR reaction, NH_3 and NO react on a 1:1 molar ratio. Thus, increased NH_3/NO_x values lead to elevated unreacted NH_3 at the SCR outlet. Unreacted NH_3 of the deNO_x process is then oxidized in the ASC (Figure 11a). The activity of the ASC is decreased at higher NH_3/NO_x ratios, leading to increased NH_3 emissions at the outlet. Despite the strong NH_3 oxidation, the ASC is characterized by high selectivity to NO_x and N_2O that becomes more important when unreacted NH_3 in the SCR is higher. NO_x conversion is maximized in the SCR due to the abundant concentrations of NH_3, while the SCR layer of the ASC catalyst counterbalances the high selectivity of NH_3 oxidation to NO, keeping NO_x concentrations at acceptable levels, compliant with Tier III

limits (<3.4 g/kWh) (Figure 11b). Concerning N_2O, limited formation is observed during SCR (minimally affected by NH_3/NO_x); however, the simultaneous oxidation of NH_3 and NO in the ASC results in important N_2O formation, especially at higher NH_3 engine-out concentrations (Figure 11c). According to Figure 11d, N_2O produced in the AOC layer corresponds to significant levels of CO_2-equivalent emissions that reach almost 500 g/kWh at high NH_3 concentrations. These levels are comparable to other low-carbon solutions, such as LNG combustion, where CO_2-equivalent emissions for low-speed two-stroke engines vary between 400 g/kWh (high-pressure dual-fuel mode) and 500 g/kWh (low-pressure dual-fuel mode) [36].

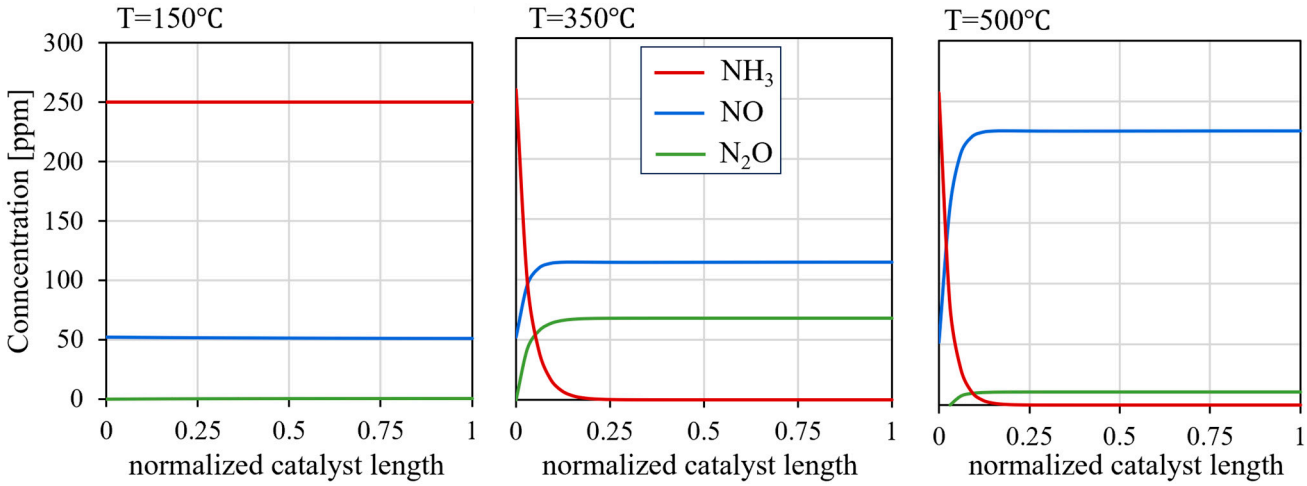

Figure 9. Concentrations of NO and N_2O as functions of axial positions along the AOC catalyst at three temperatures (150 °C, 350 °C and 500 °C).

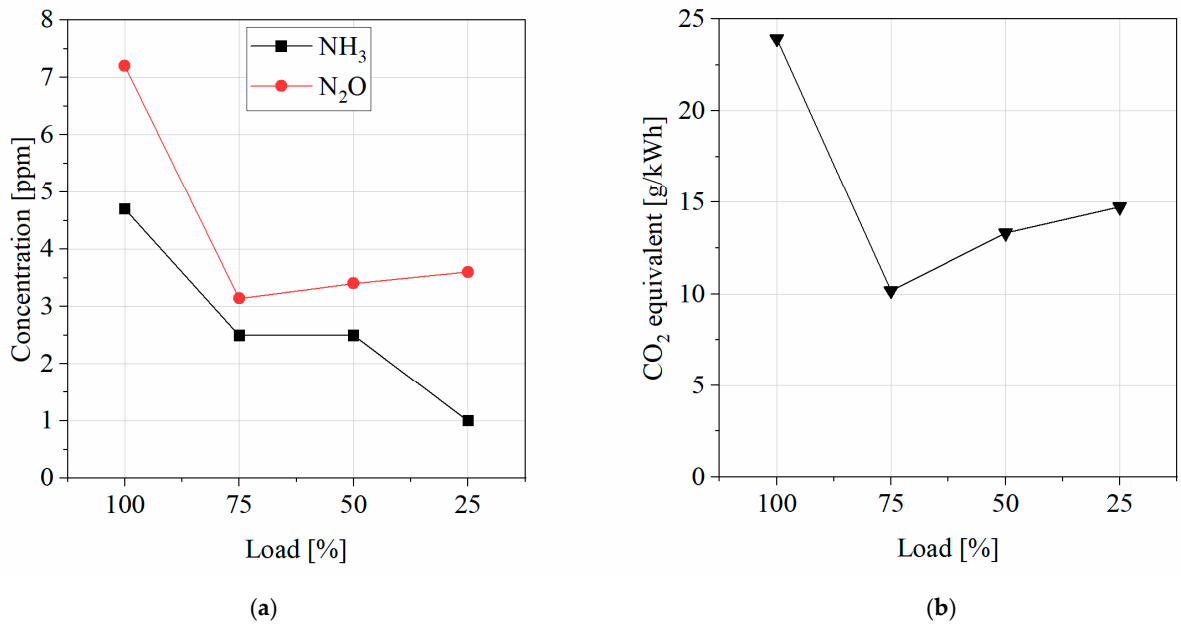

Figure 10. SCR system outlet: (**a**) NH_3 slip and N_2O selectivity; (**b**) CO_2-equivalent emissions over 100-year GWP (inlet NO_x = 2000 ppm).

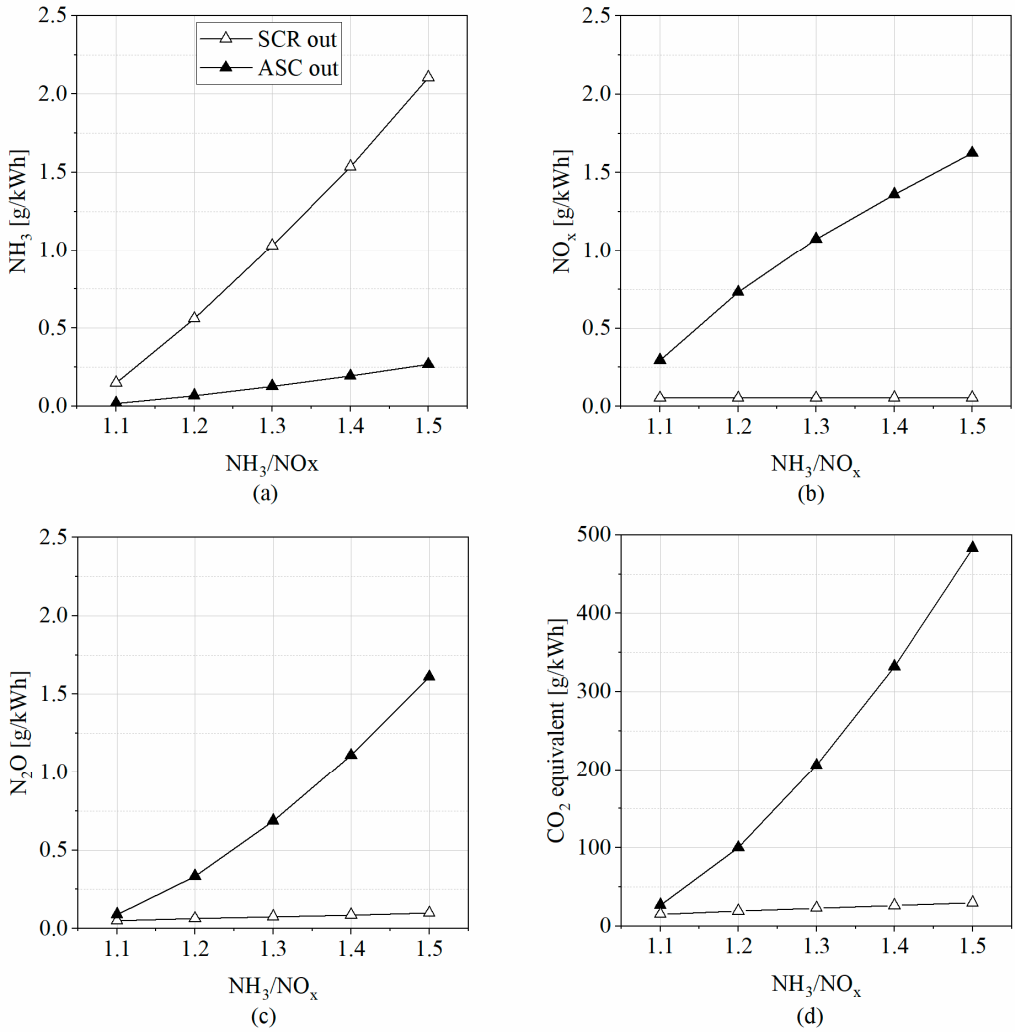

Figure 11. SCR and ASC system outlet: (**a**) NH_3, (**b**) NO_x, (**c**) N_2O and (**d**) CO_2-equivalent emissions over 100-year GWP, for various NH_3/NO_x ratios (inlet NO_x = 1500 ppm).

In addition, N_2O emissions from NH_3 in-cylinder combustion are expected to further increase the total GHG emissions. Therefore, both sources need to be considered for the successful control of N_2O emissions, eventually via a targeted additional catalyst. A different SCR layer composition could be beneficial for N_2O abatement. For example, iron-based catalysts might be a better option compared to the V-based catalyst considered here as they have the ability of simultaneous reduction of NO_x and N_2O [18]. Another possible solution is the direct reduction of N_2O through thermal decomposition [17,18,37].

4. Summary and Conclusions

The testing and simulation results of the marine engine aftertreatment models highlighted the following:

- In the case where engine-out NH_3 levels are lower than the ones required in the deNO_x process (i.e., NH_3 injection upstream of the SCR), NO_x conversion can be optimized to comply with the strictest IMO limits with minimal levels of NH_3 slip and N_2O formation.
- In the case where NH_3/NO_x is greater than 1, unreacted NH_3 of the deNO_x process can be efficiently handled with an ASC, while NO_x concentrations can be kept at acceptable levels. Concerning N_2O, NH_3 oxidation in the ASC is highly selective to N_2O formation, which is enhanced at higher NH_3 concentrations. In this case, the CO_2-equivalent emissions over a 100-year period are comparable to LNG marine engines.

Considering these indications, it is preferable to tune NH_3 combustion to ensure that NH_3/NO_x is less than 1, so as to minimize unreacted ammonia in the aftertreatment system and thus keep N_2O formed there at low levels. Except from the part produced in the catalytic aftertreatment devices, N_2O levels in the exhaust gas are expected to further increase when engine-out quantity from NH_3 combustion is considered. Therefore, the potential CO_2 benefit of NH_3 combustion may be counterbalanced, to a certain extent, due to the strong GWP of N_2O. Hence the use of NH_3 as a fuel to decarbonize the maritime sector will be beneficial only if these levels can be kept at low levels. Based on the above, an appropriate control strategy and optimization of the exhaust aftertreatment system of the NH_3 engine are of high importance as NO_x reduction should be accompanied by limited NH_3 slip and N_2O formation. For this reason, the activities of this work are further expanded with future steps including the following:

- Integration in the catalyst model of N_2O chemistry and the relevant catalytic processes in a dedicated deN_2O catalyst.
- Experimental small-scale investigation of the performance of new catalyst technologies, followed by calibration and validation of the model using the test data.
- Application of the new catalyst models in the exhaust gas stream of NH_3 engines.
- Development and optimization of the complete exhaust aftertreatment system and controls for NH_3 marine engine applications.

Author Contributions: Conceptualization, G.V., A.D. and G.K.; methodology, G.V., A.D. and G.K.; software, G.V.; validation, G.V.; writing—original draft preparation, G.V.; writing—review and editing, G.V., A.D. and G.K.; supervision, G.K. and L.N. All authors have read and agreed to the published version of the manuscript.

Funding: This work has been funded by the ENGIMMONIA project, which has received funding from the European Union's Horizon 2020 research and innovation program under grant agreement Nr. 955413.

Data Availability Statement: The data presented in this study are available in this article.

Acknowledgments: The authors would like to acknowledge support of this work by the personnel of the Laboratory of Applied Thermodynamics for performing the experimental campaign of the catalytic samples and AVL for providing the AVL Sesam i60 FT SII analyzer used in the experiments.

Conflicts of Interest: The authors declare no conflict of interest. The funders had no role in the design of the study; in the collection, analyses, or interpretation of data; in the writing of the manuscript; or in the decision to publish the results.

Nomenclature

A. Latin Letters

$\mathbf{c}$	Concentration mol/m^3
$\mathbf{C_p}$	Specific heat capacity J/(kg·K)
$\mathbf{d_h}$	Hydraulic diameter of a channel m
$\mathbf{d_{pore}}$	Mean pore size m
$\mathbf{D_{Knud}}$	Knudsen diffusivity m^2/s
$\mathbf{D_{mol}}$	Molecular diffusivity m^2/s
$\mathbf{D_w}$	Effective diffusivity m^2/s
$\mathbf{h}$	Heat transfer coefficient W/(m^2·K)
$\mathbf{k_j}$	Mass transfer coefficient m/s
$\mathbf{M}$	Molecular weight kg/mol
$\mathbf{n}$	Stoichiometric coefficient -
$\mathbf{R}$	Universal gas constant J/(mol·K)
$\mathbf{R_k}$	Reaction rate mol/(m^3·s)
$\mathbf{S}$	Source term W/m^3

$\mathbf{S_F}$	Monolith specific surface area m^2/m^3
T	Temperature K
t	Time s
v	Velocity m/s
w	Dimension perpendicular to wall surface -
$\mathbf{w_c}$	Washcoat layer thickness m
$\mathbf{y_j}$	Molar fraction -
z	Axial coordinate along monolith m
B. Greek Letters	
ΔH	Reaction heat J/mol
ε	Macroscopic void fraction -
$\varepsilon_{\mathbf{pore}}$	Porosity of the washcoat -
λ	Thermal conductivity W/m·K
ρ	Density kg/m^3
C. Subscripts and Superscripts	
g	Exhaust gas
j	Species index
k	Reaction index
s	Solid

Appendix A

This section presents supplementary equations regarding the model of the flow through the catalyst (Section 2.2.1).

A.1. 1D Model (Channel Approach)

The heat and mass transfer coefficients are calculated according to the following definitions:

$$h = \frac{Nu\times}{d_h} \tag{A1}$$

$$k_j = \frac{Sh \times D_{mol,j}}{d_h} \tag{A2}$$

The dimensionless Nusselt (Nu) and Sherwood (Sh) numbers can be calculated for the well-known correlations of laminar flow accounting for entrance effects as below:

$$Nu = 2.976\left(1 + 0.095 \times \frac{Re \times Pr \times d_h}{z}\right)^{0.45} \tag{A3}$$

$$Sh = 2.976\left(1 + 0.095 \times \frac{Re \times Sc \times d_h}{z}\right)^{0.45} \tag{A4}$$

The S term contained in the transient energy balance of the solid phase includes the convective heat transfer H_{conv} due to the gas flow in the channels and the heat release H_{react} by chemical reactions:

$$S = H_{conv} + H_{react} \tag{A5}$$

$$H_{conv} = h\left(\frac{S_F}{1-\varepsilon}\right)(T_g - T_s) \tag{A6}$$

$$H_{react} = \frac{1}{1-\varepsilon}\sum_{k=1}^{n_k} \Delta H_k R_k \tag{A7}$$

A.2. 1D+1D Model

The boundary conditions for the washcoat layer are:

$$D_{w,j}\left.\frac{\partial y_{s,j}}{\partial w}\right|_{w=-w_c} = k_j\left(y_{g,j} - \left.y_{s,j}\right|_{w=-w_c}\right) \tag{A8}$$

$$\left.\frac{\partial y_{s,j}}{\partial w}\right|_{w=0} = 0 \tag{A9}$$

where w = 0 corresponds to the wall boundary and w = $-w_c$ to the external surface of the washcoat.

The mean transport pore model used the expression

$$\frac{1}{D_{w,j}} = \frac{\tau}{\varepsilon_{pore}}\left(\frac{1}{D_{mol,j}} + \frac{1}{D_{knud,j}}\right) \tag{A10}$$

with the Knudsen diffusivity:

$$D_{knud,j} = \frac{d_{pore}}{3}\sqrt{\frac{8RT}{\pi M_j}} \tag{A11}$$

The porosity ε_{pore} and the mean pore size d_{pore} can be extracted from the microstructural properties of the washcoat, while tortuosity τ is an empirical parameter.

References

1. International Maritime Organization. *Fourth IMO GHG Study Full Report*; International Maritime Organization: London, UK, 2020.
2. Agencia Europea de Seguridad Marítima; Agencia Europea de Medio Ambiente. *EUROPEAN Maritime Transport Environmental Report*; Publications Office of the European Union: Luxembourg, 2021.
3. International Maritime Organization. *IMO(MEPC72): Resolution MEPC.304(72), Initial IMO Strategy on Reduction of GHG Emissions from Ships*; International Maritime Organization: London, UK, 2018.
4. IMO Marine Environment Protection Committee. *Eightieth Session (MEPC 80)-Summary Report*; International Maritime Organization: London, UK, 2023.
5. Ni, P.; Wang, X.; Li, H. A review on regulations, current status, effects and reduction strategies of emissions for marine diesel engines. *Fuel* **2020**, *279*, 118477. [CrossRef]
6. DNV. Energy Transition Outlook 2023. Maritime Forecast to 2050. A Deep Dive into Shipping's Decarbonization Journey. Available online: https://www.dnv.com/Publications/maritime-forecast-to-2050-2023-edition-246744 (accessed on 31 August 2023).
7. Joung, T.H.; Kang, S.G.; Lee, J.K.; Ahn, J. The IMO initial strategy for reducing Greenhouse Gas (GHG) emissions, and its follow-up actions towards 2050. *J. Int. Marit. Saf. Environ. Aff. Shipp.* **2020**, *4*, 1–7. [CrossRef]
8. Dimitriou, P.; Javaid, R. A review of ammonia as a compression ignition engine fuel. *Int. J. Hydrogen Energy* **2020**, *45*, 7098–7118. [CrossRef]
9. Rodríguez, C.G.; Lamas, M.I.; Rodríguez, J.d.D.; Abbas, A. Possibilities of Ammonia as Both Fuel and NO_x Reductant in Marine Engines: A Numerical Study. *J. Mar. Sci. Eng.* **2022**, *10*, 43. [CrossRef]
10. Lesmana, H.; Zhang, Z.; Li, X.; Zhu, M.; Xu, W.; Zhang, D. NH_3 as a transport fuel in internal combustion engines: A technical review. *J. Energy Resour. Technol.* **2019**, *141*, 070703. [CrossRef]
11. Erdemir, D.; Dincer, I. A perspective on the use of ammonia as a clean fuel: Challenges and solutions. *Int. J. Energy Res.* **2021**, *45*, 4827–4834. [CrossRef]
12. Chai, W.S.; Bao, Y.; Jin, P.; Tang, G.; Zhou, L. A review on ammonia, ammonia-hydrogen and ammonia-methane fuels. *Renew. Sustain. Energy Rev.* **2021**, *147*, 111254. [CrossRef]
13. Li, T.; Zhou, Z.; Wang, N.; Wang, X.; Chen, R.; Li, S.; Yi, P. A comparison between low- and high-pressure injection dual-fuel modes of diesel-pilot-ignition ammonia combustion engines. *J. Energy Inst.* **2022**, *102*, 362–373. [CrossRef]
14. Nova, I.; Tronconi, E. *Fundamental and Applied Catalysis Urea-SCR Technology for deNO$_x$ after Treatment of Diesel Exhausts*; Springer: Berlin/Heidelberg, Germany, 2014; Available online: http://www.springer.com/series/5964 (accessed on 31 August 2023).
15. Putluru, S.S.R.; Schill, L.; Godiksen, A.; Poreddy, R.; Mossin, S.; Jensen, A.D.; Fehrmann, R. Promoted V_2O_5/TiO_2 catalysts for selective catalytic reduction of NO with NH_3 at low temperatures. *Appl. Catal. B Environ.* **2016**, *183*, 282–290. [CrossRef]
16. Klint Torp, T.; Hansen, B.B.; Vennestrøm, P.N.R.; Janssens, T.V.W.; Jensen, A.D. Modeling and Optimization of Multi-functional Ammonia Slip Catalysts for Diesel Exhaust Aftertreatment. *Emiss. Control. Sci. Technol.* **2021**, *7*, 7–25. [CrossRef]
17. Youn, S.; Song, I.; Kim, D.H. Promotional effect on selective catalytic reduction of NO_x with NH_3 over overloaded W and Ce on V_2O_5/TiO_2 catalysts. *J. Nanomater.* **2015**, *2015*, 273968. [CrossRef]
18. Han, J.; Wang, A.; Isapour, G.; Härelind, H.; Skoglundh, M.; Creaser, D.; Olsson, L. N_2O Formation during NH_3-SCR over Different Zeolite Frameworks: Effect of Framework Structure, Copper Species, and Water. *Ind. Eng. Chem. Res.* **2021**, *60*, 17826–17839. [CrossRef]
19. Wang, A.; Wang, Y.; Walter, E.D.; Kukkudapu, R.K.; Guo, Y.; Lu, G.; Weber, R.S.; Wang, Y.; Peden, C.H.F.; Gao, F. Catalytic N_2O decomposition and reduction by NH_3 over Fe/Beta and Fe/SSZ-13 catalysts. *J. Catal.* **2018**, *358*, 199–210. [CrossRef]
20. Zhang, X.; Shen, Q.; He, C.; Ma, C.; Cheng, J.; Li, L.; Hao, Z. Investigation of selective catalytic reduction of N_2O by NH_3 over an Fe-mordenite catalyst: Reaction mechanism and O_2 effect. *ACS Catal.* **2012**, *2*, 512–520. [CrossRef]

21. Exothermia, S.A. *Exothermia Suite User Manual*, version 2022.3; Gamma Technologies, LLC: Westmont, IL, USA, 2022.
22. Karamitros, D.; Koltsakis, G. Model-based optimization of catalyst zoning on SCR-coated particulate filters. *Chem. Eng. Sci.* **2017**, *173*, 514–524. [CrossRef]
23. Zhang, D.; Yang, R.T. N_2O Formation Pathways over Zeolite-Supported Cu and Fe Catalysts in NH_3-SCR. *Energy Fuels* **2018**, *32*, 2170–2182. [CrossRef]
24. Metkar, P.; Harold, M.; Balakotaiah, V. Experimental and Kinetic Modeling Study of NH_3-SCR of NO_x on Fe-ZSM-5, Cu-chabazite and combined Fe- and Cu-zeolite monolithic catalysts. *Chem. Eng. Sci.* **2013**, *87*, 51–66. [CrossRef]
25. Mihai, O.; Widyastuti, C.; Andonova, S.; Kamasamudram, K.; Li, J.; Joshi, S.; Currier, N.; Yezerets, A.; Olsson, L. The effect of cu-loading on different reactions involved in NH_3-SCR over Cu-BEA catalyst. *J. Catal.* **2014**, *311*, 170–181. [CrossRef]
26. Scheuer, A.; Hauptmann, W.; Drochner, A.; Gieshoff, J.; Vogel, H.; Votsmeier, M. Dual layer automotive ammonia oxidation catalysts: Experiments and computer simulation. *Appl. Catal. B Environ.* **2012**, *111–112*, 445–455. [CrossRef]
27. Colomb, M.; Nova, I.; Tronconi, E.; Schmeißer, V.; Brandl-Konrad, B.; Zimmermann, L.R. Experimental Modeling Study of a dual-layer (SCR + PGM) NH_3 slip monolith catalyst (ASC) for automotive SCR aftertreatment systems. Part I. Kinetics for the PGM Component and Analysis of SCR/PGM Interactions. *Appl. Catal. B Environ.* **2013**, *142–143*, 861–876. [CrossRef]
28. Nadimi, E.; Przybyła, G.; Lewandowski, M.T.; Adamczyk, W. Effects of ammonia on combustion, emissions, and performance of the ammonia/diesel dual-fuel compression ignition engine. *J. Energy Inst.* **2023**, *107*, 101158. [CrossRef]
29. Reiter, A.J.; Kong, S.C. Combustion and emissions characteristics of compression-ignition engine using dual ammonia-diesel fuel. *Fuel* **2011**, *90*, 87–97. [CrossRef]
30. Niki, Y.; Nitta, Y.; Sekiguchi, H.; Hirata, K. Diesel fuel multiple injection effects on emission characteristics of diesel engine mixed ammonia gas into intake air. *J. Eng. Gas Turbines Power* **2019**, *141*, 061020. [CrossRef]
31. Zhu, Y.; Xia, C.; Shreka, M.; Wang, Z.; Yuan, L.; Zhou, S.; Feng, Y.; Hou, Q.; Ahmed, S.A. Combustion and emission characteristics for a marine low-speed diesel engine with high-pressure SCR system. *Environ. Sci. Pollut. Res.* **2020**, *27*, 12851–12865. [CrossRef] [PubMed]
32. Zhu, Y.; Li, T.; Xia, C.; Feng, Y.; Zhou, S. Simulation analysis on vaporizer/mixer performance of the high-pressure SCR system in a marine diesel. *Chem. Eng. Process.-Process Intensif.* **2020**, *148*, 107819. [CrossRef]
33. Christensen, S.R.; Hansen, B.B.; Pedersen, K.H.; Thøgersen, J.R.; Jensen, A.D. Selective Catalytic Reduction of NO_x over V_2O_5-WO_3-TiO_2 SCR Catalysts: A Study at Elevated Pressure for Maritime Pre-turbine SCR Configuration. *Emiss. Control Sci. Technol.* **2019**, *5*, 263–278. [CrossRef]
34. Zengel, D.; Barth, S.; Casapu, M.; Grunwaldt, J.D. The impact of pressure and hydrocarbons on NO_x abatement over Cu- and Fe-zeolites at pre-turbocharger position. *Catalysts* **2021**, *11*, 336. [CrossRef]
35. MARPOL, Annex VI—Regulations for the Prevention of Air Pollution from Ships, Appendix II—Test Cycles and Weighting Factors (Regulation 13). Available online: http://www.marpoltraining.com/MMSKOREAN/MARPOL/Annex_VI/app2.htm (accessed on 31 August 2023).
36. Pavlenko, N.; Comer, B.; Zhou, Y.; Clark, N.; Rutherford, D. *The Climate Implications of Using LNG as a Marine Fuel*; International Council on Clean Transportation: Washington, DC, USA, 2020; Available online: www.theicct.org (accessed on 31 August 2023).
37. Obalová, L. Catalytic decomposition of N_2O and NO. *Catalysts* **2021**, *11*, 667. [CrossRef]